Journal of Materials Science & Technology xxx (2018) xxx–xxx

Contents lists available at ScienceDirect

Journal of Materials Science & Technology

journal homepage: www.jmst.org

Basal-plane stacking-fault energies of Mg alloys: A first-principles study of metallic alloying effects

Qing Dong[a], Zhe Luo[a], Hong Zhu[b,*], Leyun Wang[a], Tao Ying[a], Zhaohui Jin[a], Dejiang Li[a], Wenjiang Ding[a], Xiaoqin Zeng[a,*]

[a] National Engineering Research Center of Light Alloy Net Forming and State Key Laboratory of Metal Matrix Composite, School of Materials Science and Engineering, Shanghai Jiao Tong University, Shanghai, 200240, China
[b] University of Michigan – Shanghai Jiao Tong University Joint Institute, Shanghai Jiao Tong University, Shanghai, 200240, China

ARTICLE INFO

Article history:
Received 20 December 2017
Received in revised form 27 January 2018
Accepted 28 January 2018
Available online xxx

Keywords:
First-principles calculations
Magnesium alloys
Stacking-fault energy
Alloying effect

ABSTRACT

Generalized stacking-fault energies (GSFEs) of basal-plane stacking faults I_1 and I_2 in Mg alloys have been studied based on first-principles calculations, where 43 alloying elements were considered. It is found that the most contributing features of alloying elements to GSFEs are bulk modulus, equilibrium volume, binding energy, atomic radius and ionization energy. Both bulk modulus and ionization energy exhibit positive relationships with GSFEs, and the others show opposite relationships. Multiple regressions have been performed to offer a quantitative prediction for basal-plane GSFEs in Mg-*X* systems. GSFEs, alloying effects of elements and the prediction model established within this work may provide guidelines for new Mg alloys design with better ductility.

1. Introduction

Magnesium (Mg) and its alloys are considered as promising structural materials for various applications in aerospace, automobile and microelectronics industries [1], where a reduction in weight is necessary for high energy efficiency. Mg alloys with a low mass density, which is 23% of steel and 66% of aluminum, is considered as the most lightweight structural materials. However, the potential use of Mg alloys is limited due to their low ductility and poor formability, which are due to the fact that there are only two independent slip systems on the basal plane in metals with hexagonal close packed (HCP) structures, such as Mg, far from sufficient compared to that in face centered cubic (FCC) structures. Controlling the microstructural morphology and microdefects, reducing the activation energy of basal plane slip and introducing more non-basal slip modes are important to improve the ductility of magnesium alloys.

Stacking-fault energy (SFE) is a fundamental parameter in metal and alloys, which is related to plastic deformation. Generalized stacking-fault energies (GSFEs) could be calculated along the minimum energy pathway (MEP) in a fault plane. Particularly, local minimum and maximum of GSFEs are noted as stable (or intrinsic) SFE and unstable SFE respectively. On the other hand, deformation mechanisms in HCP metals contain basal-plane and non-basal plane slip systems. The slip modes of dislocations in HCP metals are rationalized based on the GSFEs of these slip systems [2]. In other words, the slip systems with a lower GSFE would be favorable during plastic deformation. The motion of basal-plane dislocations is usually dominant in Mg alloys since the basal-plane GSFEs including SFEs of I_1 and I_2 faults are much lower than that of prismatic and pyramidal slip systems [3,4]. The nucleation of <c + a> dislocations in Mg alloys, which are the out of basal plane dislocations, were found to be activated by the basal-plane intrinsic I_1 stacking faults [5]. Basal-plane I_1 stacking fault energy was also proved to influence the behavior of <c + a> dislocations in non-basal slip systems of Mg alloys [2].

Addition of alloying elements into Mg matrices has been reported as an effective method to modify SFEs and improve ductility of Mg alloys [6]. Sandlobes et al. [5] investigated the relationship between ductility and SFEs in pure Mg and Mg-Y alloys. Their work revealed that ductility of Mg-Y alloys was enhanced by the high activity of the <c + a> dislocations as a result of the reduced SFEs of I_1 faults. Han et al. [7] revealed that basal-plane GSFEs in Mg alloys were strongly relatated to the evolution of dislocations and tunable upon doping. Their work showed that Li addition to Mg increased GSFEs and favored dislocation-mediated processes which

* Corresponding authors.
E-mail addresses: hong.zhu@sjtu.edu.cn (H. Zhu), xqzeng@sjtu.edu.cn (X. Zeng).

https://doi.org/10.1016/j.jmst.2018.02.009
1005-0302/© 2018 Published by Elsevier Ltd on behalf of The editorial office of Journal of Materials Science & Technology.

tend to generate trailing partials on basal planes, whilst Al addition decreased GSFEs and favored sequential faulting across the basal plane. Zhang et al. [8] calculated the intrinsic SFEs of basal I_2 faults with 52 solute elements in Mg-*X* alloy systems and found that intrinsic SFEs of I_2 increased with a decrease in atomic radius or increase in ionization energy of alloying elements.

Previous research mentioned above all reached a conclusion that basal-plane stacking faults play a dominating role in deformation mechanisms of Mg alloys [2–5,7,8], and a large number of alloying elements have been considered for the determinations of the intrinsic SFEs of I_2 faults [8], while few people focused on unstable SFEs of I_2 faults as well as the intrinsic and unstable SFEs of I_1 faults in alloying systems, which are of great importance for evaluating GSFEs in basal-plane slip systems and understanding the deformation mechansims in Mg alloys. In this work, we calculated intrinsic and unstable SFEs of both I_1 and I_2 faults for Mg alloys. Forty-three regular alloying elements for Mg were considered to give an informative and exhaustive GSFE database for Mg binary alloy systems, i.e., Ag, Al, Au, Ba, Be, Bi, Ca, Cd, Co, Cr, Cu, Fe, Ga, Hf, Hg, In, Ir, K, La, Li, Mn, Mo, Na, Nb, Ni, Pb, Pd, Pt, Re, Rh, Ru, Sc, Sm, Sn, Sr, Ta, Tc, Ti, Tl, V, W, Y, Zn and Zr. To understand the alloying effects on GSFEs of Mg alloys, we selected several possible properties of alloying elements and doped systems which might influence the GSFEs in Mg-*X* alloys. Statistical analyses were performed to identify the most contributing features to GSFEs. Together with basal-plane GSFEs in Mg and Mg-X alloys, the contributing properties of alloying elements to GSFEs found in this work are expected to be a useful guideline for the design of new Mg alloys with good ductility and formability.

2. Computational methods

In this work, we have chosen the growth fault I_1 and the deformation fault I_2 for basal-plane GSFE calculations in pure Mg and Mg-*X* binary alloys. According to the periodical atomic configuration in HCP structures, a perfect sequence of atomic layers could be described as ... ABABAB ..., and the growth fault I_1 could be formed by removing a basal plane in a perfect structure and then shearing the atomic layers above the fault with $\vec{b} = \frac{1}{3}\left[10\bar{1}0\right]$:

$$\ldots\text{ABABABAB}\ldots \rightarrow \ldots\text{ABABBABA}\ldots \rightarrow \ldots\text{ABABCBCB}\ldots \quad (1)$$

while the deformation fault I_2 could be formed by shearing half of the atomic layers in a perfect structure with $\vec{b} = \frac{1}{3}\left[10\bar{1}0\right]$:

$$\ldots\text{ABABABAB}\ldots \rightarrow \ldots\text{ABABCACA}\ldots \quad (2)$$

With the stacking faults introduced to the perfect structure, the generalized stacking-fault energies could be calculated using the following equation:

$$\gamma_{GSF} = \frac{E_{GSF} - E_0}{A} \quad (3)$$

where γ_{GSF} represents the GSFE of a stacking fault structure, E_{GSF} represents the energy of the stacking faulted structure, E_0 represents the energy of a perfect structure, and A represents the surface area of the faulting plane.

Density functional theory (DFT) calculations were performed within the Vienna Ab-initio Simulation Package (VASP) [9–11]. The generalized-gradient-approximation (GGA), Perdew-Burke-Ernzerhof (PBE) exchange-correlation functional and projector augmented wave method (PAW) were used [12–14].

The (0001) Mg slab with 12 atomic layers and 2×2 primitive cell along surface plane was adopted in our simulations for pure Mg and Mg-*X* binary alloys, as illustrated in Fig. 1. To avoid the interactions between adjacent images, 15 Å vacuum was employed along the [0001] direction. In the cases of Mg-*X* systems, one Mg atom in the 6th layer near the stacking-fault plane was substituted with an *X* atom, corresponding to the doping concentration of 25.0 at.% on the doping plane and 1.1 at.% in the entire Mg-*X* systems. To calculate the GSFEs of the I_2 faults, a generalized stacking fault pathway was built from a perfect slab to an I_2 faulted slab, in which the I_2 faulted slab was formed by shearing half of the atomic layers in a perfect slab with the Burger vector $\vec{b} = \frac{1}{3}\left[10\bar{1}0\right]$, as shown in Fig. 1(a,b). To calculate the GSFEs of the I_1 faults, a generalized stacking fault pathway was built from an I_1 faulted slab to an I_1' faulted slab, during which the position of faulting plane has climbed from one atomic layer to an adjacent layer. In this procedure, the two faulted slabs I_1 and I_1', shown in Fig. 1(c,d), represented similar faulted structures both with I_1 faults but located on different atomic layers. The bottom half atomic layers in an I_1 faulted slab were shifted a Burgers vector $\vec{b} = \frac{1}{3}\left[10\bar{1}0\right]$ to form an I_1' faulted slab, and the two endpoints of the fault pathway, I_1 and I_1' structures, were expected to exhibit similar stacking-fault energies. The climbing-image nudged elastic band (CINEB) methods [15] were used to compute GSFE curves along the MEP and to acquire GSFE at saddle point as the unstable SFE. In our simulations, *k*-point meshes of $8 \times 8 \times 1$ Γ-centered grids and a convergence criterion of force of 0.01 eV/Å were used.

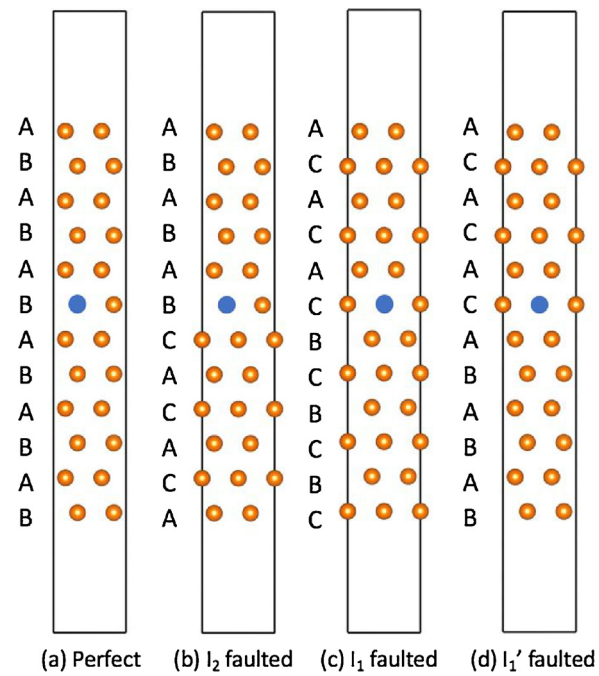

Fig. 1. Atomic configuration of (a) perfect, (b) I_2 faulted, (c) I_1 faulted and (d) I_1' faulted (0001) $Mg_{47}X$ slab. Each faulted slab contains a stacking-fault interface in the middle, where the local atomic configuration is FCC-like.

3. Results

3.1. Formation energy and binding energy of $Mg_{47}X$ structures

Formation energy and binding energy of $Mg_{47}X$ structures were computed and shown in Table 1. The formation energy of a $Mg_{47}X$ slab is the energy required to substitute a Mg atom with an *X* atom in a perfect Mg_{48} slab, which can be determined based on the equation below:

$$E_f(Mg_{47}X) = E_{slab}(Mg_{47}X) - E_{slab}(Mg_{48}) + E_{bulk}(Mg) - E_{bulk}(X) \quad (4)$$

where E_{slab} represents the total energy of a perfect slab without any stacking faults, E_{bulk} represents the atomic energy of the metallic element in its stable bulk structure, which were acquired from

Table 1
Basal-plane GSFEs in Mg-*X* binary alloying systems, together with properties of alloying element *X* and $Mg_{47}X$ slabs. Properties of $Mg_{47}X$ structures are the formation energy (E_f) and binding energy (E_b) for Mg-*X* alloying systems. Intrinsic and unstable GSFEs of I_1 and I_2 faults are noted as γ_{I_1}, γ_{us_1}, γ_{I_2} and γ_{us_2}. Properties of alloying elements are the atomic radius (R), 1st and 2nd ionization energy (E_{i_1} and E_{i_2}) [17], number of valence electrons (N_{ve}), equilibrium volume (V_{hcp}) and equilibrium bulk modulus (κ_{hcp}) [18] for HCP structures of alloying elements.

Alloying element	E_f	E_b	γ_{I_1}	γ_{us_1}	γ_{I_2}	γ_{us_2}	R[17]	E_{i_1} [17]	E_{i_2} [17]	N_{ve}	V_{hcp}[18]	κ_{hcp}[18]
	(eV)	(eV)	(mJ/m^2)	(mJ/m^2)	(mJ/m^2)	(mJ/m^2)	(pm)	(mJ/mol)	(mJ/mol)		(Å3/atom)	(GPa)
Mg	0.00	0.00	16.1	86.9	37.6	89.6	160	738	1451	2	22.89	35.7
Li	−0.20	−0.26	18.1	95.6	47.6	97.5	152	520	7298	1	20.33	13.5
Be	1.24	−0.90	25.8	80.7	45.4	85.4	111	899	1757	2	7.92	121.1
Na	0.32	0.79	16.8	79.3	38.3	80.4	186	496	4562	1	37.18	7.6
Al	0.02	−1.93	13.1	86.0	21.3	86.3	143	578	1817	3	16.75	70.8
K	1.58	2.27	10.7	22.9	6.9	28.1	179	419	3051	1	74.02	3.5
Ca	0.10	−0.25	17.0	58.3	28.7	61.6	195	590	1145	2	41.93	17.7
Sc	−0.18	−2.96	17.0	91.7	34.6	94.5	210	631	1235	3	24.47	54.9
Ti	0.68	−3.21	2.3	108.7	22.4	106.9	147	658	1310	4	17.29	112.8
V	1.05	−3.11	18.0	117.2	50.2	120.5	134	650	1414	5	13.84	173.2
Cr	1.11	−5.42	19.7	115.6	48.4	118.8	128	653	1592	6	11.94	233.5
Mn	0.84	−1.61	12.1	110.2	37.5	111.5	127	717	1509	7	10.75	279.7
Fe	1.17	−2.46	−1.3	68.6	27.0	101.9	126	759	1561	8	10.18	288.3
Co	0.83	−2.98	23.4	113.8	63.5	119.0	125	758	1646	9	10.85	212.5
Ni	0.36	−3.41	24.7	100.4	63.2	106.8	124	737	1753	10	10.95	193.8
Cu	0.56	−1.75	21.1	86.6	50.5	90.9	128	745	1958	1	12.04	136.1
Zn	−0.07	0.38	17.6	79.5	32.7	82.1	134	906	1733	2	15.40	51.8
Ga	−0.20	−1.45	9.5	79.8	22.4	79.0	135	579	1979	3	19.18	45.9
Sr	0.72	0.66	16.7	32.9	15.6	30.1	215	549	1064	2	54.72	11.4
Y	−0.13	−2.75	15.6	69.9	26.4	74.7	180	616	1181	3	32.67	40.8
Zr	0.16	−4.73	−0.4	94.8	17.5	92.2	160	660	1267	4	23.44	95.3
Nb	0.86	−4.57	−6.0	113.0	19.9	110.5	146	664	1382	5	18.90	162.8
Mo	1.34	−3.37	4.8	132.0	42.7	132.9	139	685	1558	6	16.29	233.8
Tc	0.93	−4.57	16.9	145.3	63.0	147.9	136	702	1472	7	14.63	296.1
Ru	0.12	−6.19	22.7	147.4	72.6	151.3	134	711	1617	8	13.88	309.4
Rh	−0.90	−5.40	24.7	130.3	70.9	136.1	134	720	1744	9	14.26	251.1
Pd	−1.34	−3.50	23.1	111.9	64.0	120.0	137	805	1875	10	15.60	163.6
Ag	−0.43	−1.36	17.8	93.9	48.6	97.1	144	731	2073	1	18.01	91.1
Cd	−0.31	0.50	14.0	109.9	32.5	83.9	149	868	1631	2	23.00	35.8
In	−0.15	−1.11	7.4	75.0	16.9	74.8	167	558	1821	3	27.80	34.4
Sn	−0.51	−2.11	4.0	71.8	11.9	71.9	151	709	1412	4	27.79	47.6
La	0.28	−1.60	15.9	30.2	2.5	39.4	183	538	1067	3	37.26	26.1
Sm	−0.01	−2.93	16.1	62.2	18.9	61.5	180	543	1086	8	33.91	35.7
Hf	0.50	−4.43	0.0	98.1	16.0	96.0	159	680	1440	4	22.41	109.1
Ta	1.38	−5.41	−8.2	116.3	14.3	112.0	146	761		5	18.77	188.0
W	2.04	−4.72	1.4	136.5	36.5	136.8	139	770		6	16.62	274.3
Re	1.65	−4.63	15.5	154.9	57.9	156.7	137	760		7	14.99	366.8
Ir	−0.70	−6.71	26.9	134.4	71.4	141.2	136	880	880	9	14.68	339.0
Pt	−1.71	−5.62	24.6	103.6	65.8	110.6	139	870	1791	10	15.94	235.2
Au	−1.21	−2.64	17.5	84.6	46.0	89.6	144	890	1980	1	18.22	135.0
Hg	−0.55	0.82	9.6	73.2	23.7	76.6	151	1007	1810	2	30.75	9.5
Tl	0.05	−0.57	2.7	68.7	14.8	67.7	170	589	1971	3	31.25	27.2
Pb	−0.08	−1.61	1.8	67.5	11.6	67.0	175	716	1450	4	31.81	40.2
Bi	−0.34	−1.35	−4.3	53.7	−2.6	57.0	155	703	1610	5	31.73	52.0

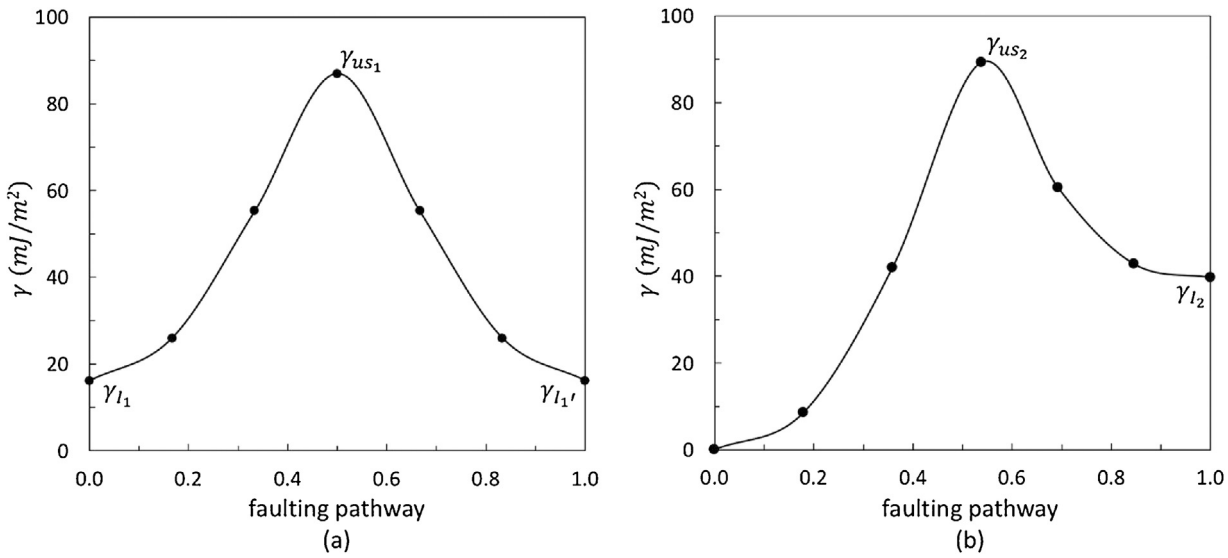

Fig. 2. GSFE curve along the faulting pathway (a) from I_1 to I_1' faulted slabs and (b) from perfect to I_2 faulted slabs. The maximum γ value along I_1 to I_1' and perfect to I_2 pathways are denoted as γ_{us_1} and γ_{us_2}.

Materials Project [16]. The formation energy (E_f) of $Mg_{47}X$ slab is in the unit of eV.

We have also determined the binding energy of a $Mg_{47}X$ slab, which is the energy required to assemble the whole slab with isolated Mg and X atoms, as shown in the following equation:

$$E_b(Mg_{47}X) = E_{slab}(Mg_{47}X) - E_{slab}(Mg_{48}) + E_{isolated}(Mg) - E_{isolated}(X) \quad (5)$$

where $E_{isolated}$ represents the energy of an isolated metal atom in vacuum. The binding energy (E_b) is shown with respect to that of pure Mg slab and in the unit of eV.

As seen from Table 1, formation energy of Mg-X structures varied from −1.71 eV (Mg-Pt) to 2.04 eV (Mg-W), and binding energies of Mg-X structures varied from −6.71 eV (Mg-Ir) to 2.27 eV (Mg-K). From Table 1, an increasing tendency of binding energy (E_b) with respect to the atomic radius (R) of alloying elements could be acquired, while for the formation energy there was no such relationships. To understand their contributions to the variation of GSFEs in Mg-X systems, statistical analysis and discussions were carried out and shown later in Section 4.2.

3.2. Generalized stacking fault energy curves for I_1 and I_2 faults in pure Mg

The fully optimized GSFE curve (γ-curve) along the faulting pathway from a perfect slab to an I_2 faulted slab, as well as that from an I_1 faulted slab to an I_1' faulted slab, are plotted in Fig. 2. Along the minimum energy path, γ_{I_1}, $\gamma_{I_1'}$ and γ_{I_2} represent the intrinsic stacking-fault energy of I_1, I_1' and I_2 faults, respectively, while γ_{us_1} and γ_{us_2} are the unstable stacking-fault energy along these two faulting pathways. In Fig. 1, since I_1 and I_1' faulted slabs were two simulation structures with the center position of local I_1 faults on adjacent atomic layers, the values of $\gamma_{I_1'}$ should be almost the same as that of γ_{I_1}.

Fig. 2 indicates that unstable SFEs give energy barrier of I_1 and I_2 faults, which were the maximum GSFE values on γ-curves along MEPs, near the middle point of the transition process where the Burgers vector $\vec{b} = \frac{1}{6}\left[10\bar{1}0\right]$. As the energy barrier describes the energy required for the transition process between two endpoints of a reaction, in this case, γ_{us_1} gives the required energy for a Mg slab to transform from an I_1 faulted structure to an I_1' faulted structure, and similarly, γ_{us_2} gives the required energy for a Mg slab to transform from a perfect structure to an I_2 faulted structure. The intrinsic SFEs at the endpoints of the γ-curves correspond to the stable stacking-fault energy of I_1 (or I_1') faulted and I_2 faulted structures.

The intrinsic and unstable stacking-fault energies of I_1 and I_2 in pure Mg structure are summarized in Table 2, together with some data in literature for comparison. From the GSFE data from this work and literature in Table 2, we note that the values of γ_{I_2} are usually about twice that of γ_{I_1}, and values of γ_{us_1} were only slightly smaller than that of γ_{us_2}. CINEB-calculations for γ-curves of I_1 and I_2 in alloying systems were also performed, and values for GSFEs are shown in Table 1, from which similar relationships between γ_{I_1} and γ_{I_2} were observed.

3.3. Intrinsic and unstable stacking-fault energies of I_1 and I_2 in $Mg_{47}X$ structures

As alloying elements were added into Mg slab, there was a variation in basal-plane GSFEs of Mg-X system due to the alloying effects. Calculated γ_{I_1} $\left(\gamma_{I_1'}\right)$, γ_{us_1}, γ_{I_2} and γ_{us_2} values in Mg-X systems given in Table 1 were plotted in Fig. 3 with respect to atomic radius of alloying elements X. A negative relationship between

Table 2
Calculated basal-plane GSFEs in pure Mg with CINEB-DFT methods (in units of mJ/m^2).

	data source	γ_{I_1} $\left(\gamma_{I_1'}\right)$	γ_{us_1}	γ_{I_2}	γ_{us_2}
Mg	This work	16.1	86.9	37.6	89.6
	Previous DFT work	18 [7]; 18 [19]; 17.1 [20]; 20 ± 1 [5]; 16 [21]; 17.98 [22]; 17.8 [23]	90 [7]; 86.2 [20]	33 [7]; 36 [19]; 36 [24]; 33.8 [20]; 30 [25]; 35 [26]; 30 [21]; 33.84 [22]; 38.3 [23]	92 [7]; 92[24] 87.6 [20]; 84.8 [25]; 86 [26]

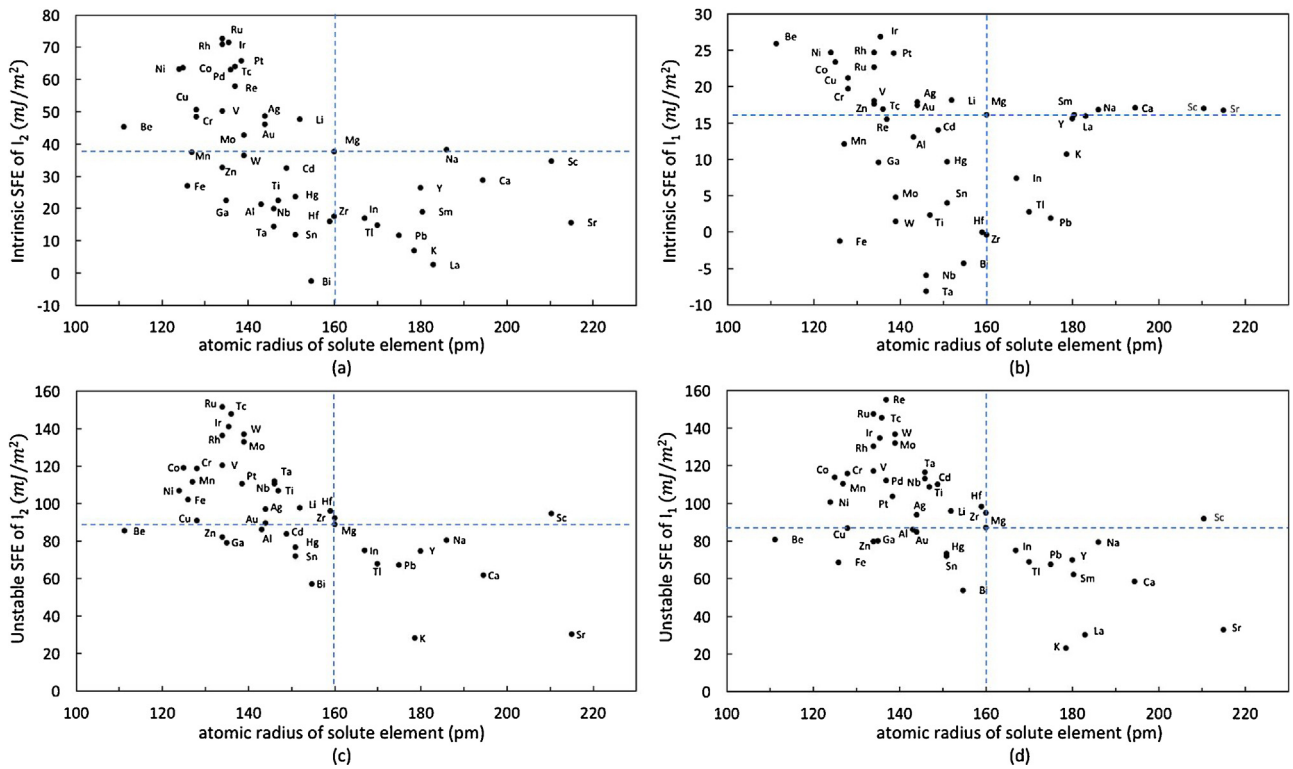

Fig. 3. Variation of calculated GSFEs including (a) intrinsic SFE of I_2, (b) intrinsic SFE of I_1, (c) unstable SFE of I_2 and (d) unstable SFE of I_1, with respect to atomic radius of alloying elements. The doping concentration is 25 at.% in doping plane and 2.08 at.% in Mg-*X* system.

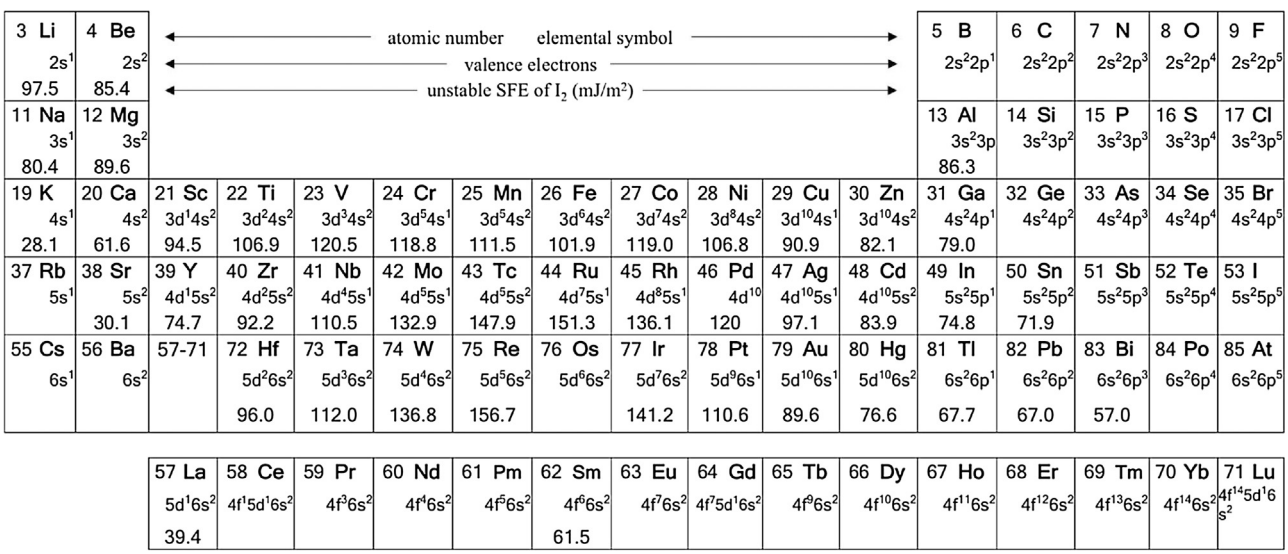

Fig. 4. Periodic table with valence electron configuration and unstable SFEs of I_2 of Mg-*X* alloying systems.

GSFEs and atomic radius of alloying elements could be observed in Fig. 3, and the range of variations of GSFEs in Mg-*X* systems could also be acquired through Table 1 and Fig. 3. Comparing to intrinsic SFEs, the variations of unstable SFEs of I_1 as well as I_2 were more strongly influenced by the alloying elements, and variations of intrinsic SFE of I_2 were more strongly influenced than instrinsic SFEs of I_1. For unstable SFEs of I_1 and I_2 faults, the variation tendency and strength of the dependence on alloying elements were similar. Intrinsic SFEs of I_1 varied from −8.2 mJ/m^2 (Mg-Ta) to 26.9 mJ/m^2 (Mg-Ir), while unstable SFEs of I_1 varied from 22.9 mJ/m^2 (Mg-K) to 154.9 mJ/m^2 (Mg-Re). In the case of I_2 faults, intrinsic SFEs varied from −2.6 mJ/m^2 (Mg-Bi) to 72.6 mJ/m^2 (Mg-Ru) and unstable SFEs varied from 28.1 mJ/m^2 (Mg-K) to 156.7 mJ/m^2 (Mg-Re). Among 43 alloying elements, Al, Bi, Ga, Hg, In, K, La, Pb, Sm, Sn, Tl and Y reduced GSFEs in Mg-*X* alloys, while Ag, Co, Cr, Ir, Li, Ni, Pd, Pt, Rh, Ru, Tc and V increased GSFEs. A detailed discussion on how alloying elements affect SFEs will be provided in Section 4.2.

4. Discussion

4.1. Relationships between γ_{I_1} and γ_{I_2} in Mg-X systems

To find out the relationships between γ_{I_1} and γ_{I_2}, further statistical analysis was performed. Pearson Correlation Coefficient was

chosen for evaluating the linear relationship between variables X and Y:

$$r(X, Y) = \frac{\mathrm{cov}(X, Y)}{\sigma_X \sigma_Y} \tag{6}$$

where $\mathrm{cov}(X, Y)$ represents the covariance between X and Y, and σ_X, σ_Y represents the standard deviations for X and Y, respectively. Pearson Correlation Coefficient r is a number in the range of $[-1, 1]$ to measure strength and direction of the linear relationship between two variables, and a larger absolute value of r indicates a stronger relationship between the variables.

Calculations performed through Eq. (6) gives the correlation coefficient $r\left(\gamma_{I_1}, \gamma_{I_2}\right) = 0.73$. It should be noted that the correlation coefficient value of 0.73 indicates a strong positive relationship between SFEs of I_1 and I_2. We also calculated the correlation coefficients $r\left(\gamma_{I_2}, \gamma_{us_2}\right) = 0.76$, and $r\left(\gamma_{us_1}, \gamma_{us_2}\right) = 0.97$.

As shown in Fig. 1, the atomic configuration at the stacking-fault interface of I_1 and I_2 faults forms local FCC-like layer structure (ABC) inside HCP layer structure (AB). The local FCC stacking introduces a characteristic stacking-fault energy, which arises from changes in the second-neighbour sequences of the planes. Although the atomic-configuration changes from HCP to local FCC exist in both I_1 and I_2 faults, there are only one such change in I_1 but two in I_2, leading to an approximated relationship of $\gamma_{I_1} = \frac{1}{2}\gamma_{I_2}$ [27]. The values of $\gamma_{I_1}/\gamma_{I_2}$ rate for Mg-X systems are calculated, and the average value of $\gamma_{I_1}/\gamma_{I_2}$ equals to 0.53, in agreement with the approximated relationship of 0.5.

4.2. Contributing factors to γ_{us_2} in $Mg_{47}X$ structure

To figure out possible factors that may contribute to the variations of GSFEs in Mg-X alloying systems, we have obtained the atomic radius (R), 1st and 2nd ionization energy (E_{i_1} and E_{i_2}) [17], number of valence electrons (N_{ve}), and the equilibrium volume (V_{hcp}) and bulk modulus (κ_{hcp}) for HCP structures of alloying elements [18], formation energy for Mg-X alloying systems (E_f) and binding energy for Mg-X alloying systems (E_b), as shown in Table 1. A periodic table with unstable SFEs of I_2 was also provided to exhibit the relation between the valence electron configuration and GSFEs in Mg-X alloying systems, as shown in Fig. 4. According to Table 1 and Fig. 4, one can see that alloying elements with more valence electrons would increase the GSFEs in Mg-X alloys.

For further statistical analysis to figure out the contributing factors to the variations of basal-plane GSFEs in Mg-X systems, unstable SFE of I_2 (γ_{us_2}) is selected as a representative for the intrinsic and unstable SFEs of I_1 and I_2, since strong positive linear relationships among these 4 basal-plane GSFE variables in Mg-X systems were achieved in Section 4.1. Multiple correlation matrix between γ_{us_2} and the selected properties of alloying elements as well as Mg-X alloying systems was computed, as shown in Table 3.

Table 3
Correlation matrix between γ_{us_2} and properties of alloying element X and Mg-X systems.

	γ_{us_2}	κ_{hcp}	V_{hcp}	E_b	R	E_{i_1}	E_f
γ_{us_2}	1	0.87	−0.77	−0.76	−0.65	0.41	0.16
κ_{hcp}	0.87	1	−0.65	−0.77	−0.65	0.39	0.28
V_{hcp}	−0.77	−0.65	1	0.58	0.80	−0.57	0.01
E_b	−0.76	−0.77	0.58	1	0.40	−0.24	−0.03
R	−0.65	−0.65	0.80	0.40	1	−0.58	−0.12
E_{i_1}	0.41	0.39	−0.57	−0.24	−0.58	1	−0.24
E_f	0.16	0.28	0.01	−0.03	−0.12	−0.24	1

Seen from Table 3, the ranking of most possible properties that contribute to basal-plane GSFEs is κ_{hcp}, V_{hcp}, E_b, R, E_{i_1} and then E_f. The positive values of correlation coefficients between κ_{hcp} and E_{i_1} and γ_{us_2} in Mg-X binary alloying systems indicate that the addiction of alloying elements with lower bulk modulus or lower 1 st ionization energy would decrease GSFEs in Mg-X alloy. In contrast, negative correlation coefficients indicate that alloying elements with larger equilibrium volume, higher binding energy or larger atomic radius would decrease GSFEs. The absolute value of correlation coefficient between E_f and γ_{us_2} is too small to convince a certain relationship between formation energy of alloying elements and GSFEs. It should be noted that R and V_{hcp} both describe the size feature of alloying elements, and the correlation coefficient between R and $V_{hcp}^{1/3}$ is 0.87, which indicates a strong positive linear relationship between these two factors, thus in further analysis atomic radius of alloying elements has be left out to avoid double-counting.

To get a visual representation of relationships between γ_{us_2} and the most contributing factors κ_{hcp}, V_{hcp} and E_b, several scatter charts were plotted with the vertical axis of γ_{us_2} and the horizontal axis of κ_{hcp}, V_{hcp}, and E_b respectively, as shown in Fig. 5, in which we could see how these three factors influence the basal-plane GSFEs in Mg-X binary systems. It could be concluded that alloying elements with lower bulk modulus would be favorable as solute addition to reduce GSFEs in Mg alloys. We also noted that alloying elements with larger equilibrium volumes would be better choices to reduce GSFEs in Mg alloys. GSFEs also varied with the binding energy E_b, and Mg-X structures with higher binding energies tended to have a lower GSFE. In summary, addition of alloying elements with lower κ_{hcp}, larger V_{hcp}, and higher E_b to $Mg_{47}X$ slabs would exhibit lower GSFEs, which means the binary alloying system would yield a better ductility.

Two alloying elements, Ni and K, are selected to explain the alloying effects of these dominating factors mentioned above. From Table 1, taking unstable SFE of I_2 as an

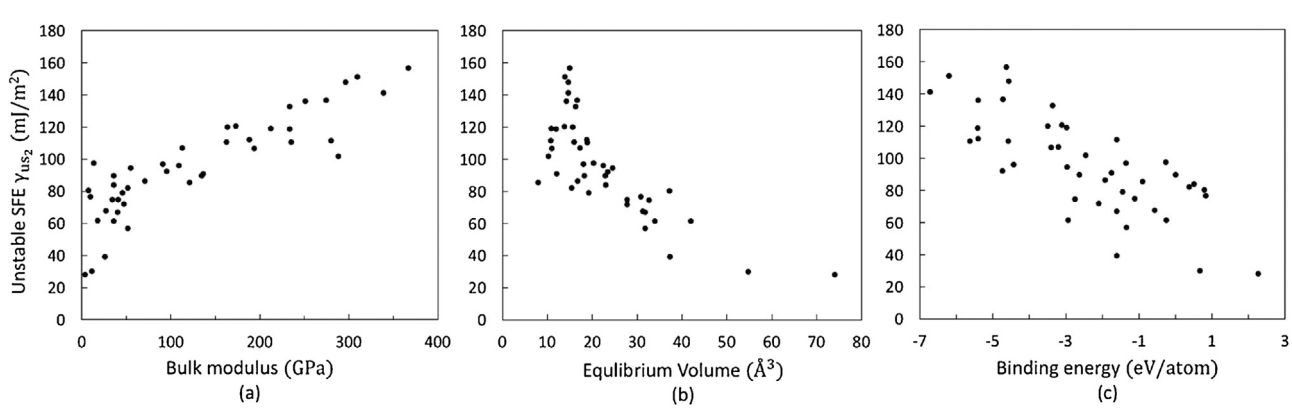

Fig. 5. Variation of calculated unstable SFE of I_2 with respect to (a) bulk modulus of alloying elements, (b) binding energy of $Mg_{47}X$ structures and (c) HCP volumes of alloying elements. γ_{us_2} values are marked with vertical axis, and κ_{hcp}, V_{hcp} and E_b values are marked with horizontal axis.

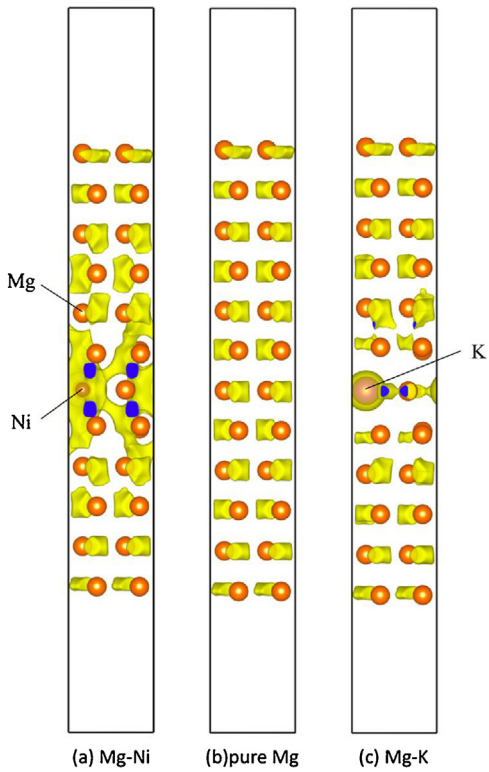

Fig. 6. Charge density iso-surface figures of perfect slabs for (b) pure Mg and Mg alloyed with Ni (a) and K (c). The yellow color indicates a high electron density and the blue color indicates a low electron density. The doping concentration is 25 at.% in doping plane and 2.08 at.% in Mg-*X* system.

example, $\gamma_{us_2}(Mg_{48}) = 89.6 mJ/m^2$, $\gamma_{I_2}(Mg_{47}Ni) = 106.8 mJ/m^2$, $\gamma_{I_2}(Mg_{47}K) = 28.1 mJ/m^2$, which means Ni-alloying increases the basal-plane GSFEs and K-alloying decreases GSFEs remarkably. Seen from Table 1, element Ni with small *R*, small V_{hcp}, high κ_{hcp} and low E_b, compared to those of Mg, raises the basal-plane GSFE values, while alloying element K with large *R*, large V_{hcp}, low κ_{hcp} and high E_b lowers GSFEs in the magnesium binary alloying systems, which also gives a convincing proof for the relationships we concluded above.

The charge density iso-surfaces of Mg-Ni, Mg-K and pure Mg are shown in Fig. 6. It is illustrated that in the Ni alloyed Mg slab, the charge density near doping plane is increased, which indicates that electrons are attracted to alloying atom Ni. This would lead to a higher GSFE value since there are more electron redistributions within the stacking-fault plane during the formation of an I_1 or I_2 fault. In addition, distance between adjacent atomic layers near Ni doped plane is decreased, which makes it difficult for the formation of local FCC structures in I_1 and I_2 faulted slabs, where a larger atomic layer separation is needed. In fully-relaxed pure Mg slab structures, the distance between the 6th and 8th atomic layers (Fig. 1) is 5.187Å for a perfect slab, 5.215Å for an I_2 faulted slab, and 5.216Å for an I_1 faulted slab, which indicates that local FCC structures are formed around stacking-fault planes with a slightly bigger layer distance than perfect HCP structure, thus the formation of local FCC structure is favored with an expanded atomic layer separation. In contrast to Ni-alloying, K-alloying expels surrounding electrons and increases the layer distance around the doping plane, and thus decreases GSFEs. Thus, from this aspect, we can also note that alloying element with smaller atomic size and stronger binding energy to Mg usually will display larger GSFEs.

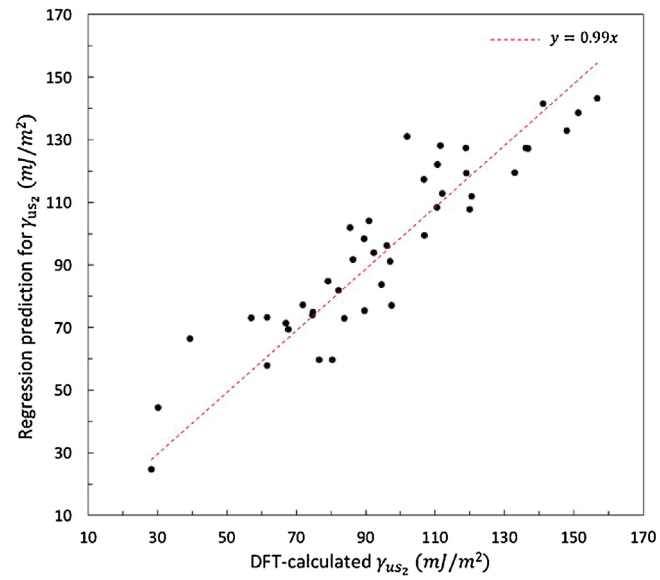

Fig. 7. Regression prediction for γ_{us_2} in Mg-*X* systems. The red dotted line is the trend line for prediction values, $y = 0.99x$, and a perfect prediction should be $y = x$. (For interpretation of the references to colour in this figure legend, the reader is referred to the web version of this article.)

4.3. Multiple regression analysis for γ_{us_2} predictions

According to Section 4.2, the most contributing properties for multiple regression analysis are κ_{hcp}, V_{hcp}, E_b and E_i, which have strong linear relationsihps with γ_{us_2}. A multiple regression equation was established to predict the unstable stacking-fault energies of I_2 in Mg-*X* systems:

$$\gamma_{us_2} = c_1 + c_2\kappa_{hcp} + c_3V_{hcp} + c_4E_b + c_5E_{i_1} \quad (7)$$

where c_1, c_2, c_3, c_4 and c_5 are the linear coefficients for multiple regression. These coefficients were acquired through calculations, $c_1 = 98.21$, $c_2 = 0.16$, $c_3 = -0.88$, $c_4 = -1.84$, $c_5 = -0.01$. Since variables in different terms of Eq. (7) are not in the same unit, where κ_{hcp} is in GPa, V_{hcp} is in $Å^3$, E_b is in eV and E_{i_1} is in kJ/mol, the coefficients of each term are not standardized, and they could only give numerical expressions of the approximation equation instead of how these factors contribute to γ_{us_2}. With the solved values of linear coefficients, Eq. (7) was used to predict the values for γ_{us_2} with κ_{hcp}, V_{hcp}, E_b and E_{i_1} of Mg-*X* systems. To visualize the goodness of fit of this prediction equation, predicted γ_{us_2} values with respect to DFT-calculated γ_{us_2} values was plotted in Fig. 7. The goodness of fit of prediction values to DFT-calculated values could be explained using the multiple correlation coefficient between the predicted values and DFT-calculated values for γ_{us_2}, which could be noted as $r\left(pre.\gamma_{us_2}, cal.\gamma_{us_2}\right) = 0.92$, and the square of correlation coefficient $r^2 = 0.84$. The high coefficient value indicates a strong equality relationship between the equation-predicted and DFT-calculated γ_{us_2} values, and the high r^2 value also indicates that 84% of γ_{us_2} values could be explained using the prediction with κ_{hcp}, V_{hcp}, E_b and E_{i_1}.

As mentioned before, Mg alloys with lower basal-plane GSFEs could activate non-basal slips and therefore show better ductility. Also through the correlation matrix analysis, we have figured out the ranking of most contributing properties of alloying elements that affect GSFEs in Mg-*X* systems, and the ranking should be in the order of κ_{hcp}, V_{hcp} and E_b. Thus this ranking would help give some guidance for new alloys design, i.e. in order to achieve better ductility, alloying elements with lower bulk modulus, larger equilibrium

volume and higher binding energy in Mg alloys would be favored as the solute addition. Moreover, bulk modulus takes the most important role among all the properties of alloying elements, and should be taken into first consideration during materials design. Furthermore, the multiple regression analysis offered a quantitative prediction for the basal-plane GSFE values in Mg-*X* systems, which could help predict ductility properties of new Mg alloys by calculating GSFEs with the known properties of alloying elements.

5. Conclusions

In summary, according to DFT-calculated GSFEs of basal-plane stacking faults in binary Mg alloys, addition of alloying elements with various properties including bulk modulus, atomic radius, ionization energy and binding energy led to a large variation of GSFEs. Alloying elements including Al, Bi, Ga, Hg, In, K, La, Pb, Sm, Sn, Tl and Y among 43 metallic elements reduced the basal-plane GSFEs in Mg alloys, whilst Ag, Co, Cr, Ir, Li, Ni, Pd, Pt, Rh, Ru, Tc and V increased the GSFEs. Linear relationships between intrinsic and unstable SFEs for basal planes as well as the numerical relationship of $\gamma_{I_1} = \frac{1}{2}\gamma_{I_2}$ were confirmed. Among the properties of alloying elements and Mg-*X* structures, the variation of basal-plane GSFEs were found strongly related to κ_{hcp}, V_{hcp}, E_b, R, E_{i_1} and E_f. The alloying elements with lower bulk modulus, larger equilibrium volume, higher binding energy, larger atomic radius, lower 1 st ionization energy would reduce the GSFEs in Mg-*X* alloys. A prediction model for basal-plane GSFEs in Mg alloys was also built to give quantitative predictions for GSFEs in new Mg alloys, which offer guidance for new Mg alloys design with better ductility.

Acknowledgements

This work is financially supported by the National Key Research and Development Program of China (No. 2016YFB0701202) and the National Natural Science Foundation of China (General Program No. 51474149 and Key Program No. 51631006). First-principles calculations were carried out with computational resources from Shanghai Jiao Tong University Super Computer Center. The authors would like to thank W.K. Qian for the helpful discussions on data analysis.

References

[1] A.H. Feng, Z.Y. Ma, Acta Mater. 57 (2009) 4248–4260.
[2] D. Rodney, L. Ventelon, E. Clouet, L. Pizzagalli, F. Willaime, Acta Mater. 124 (2016) 633–659.
[3] Z. Pei, L.F. Zhu, M. Friák, S. Sandlöbes, J. Von Pezold, H.W. Sheng, C.P. Race, S. Zaefferer, B. Svendsen, D. Raabe, J. Neugebauer, New J. Phys. 15 (2013) 043020.
[4] C. Wang, H.Y. Wang, H.Y. Zhang, X.L. Nan, E.S. Xue, Q.C. Jiang, J. Alloys Compd. 575 (2013) 423–433.
[5] S. Sandlöbes, M. Friák, S. Zaefferer, A. Dick, S. Yi, D. Letzig, Z. Pei, L.F. Zhu, J. Neugebauer, D. Raabe, Acta Mater. 60 (2012) 3011–3021.
[6] A. Datta, U. Ramamurty, S. Ranganathan, U.V. Waghmare, Comput. Mater. Sci. 37 (2006) 69–73.
[7] J. Han, X.M. Su, Z.-H. Jin, Y.T. Zhu, Scr. Mater. 64 (2011) 693–696.
[8] J. Zhang, Y. Dou, G. Liu, Z. Guo, Comput. Mater. Sci. 79 (2013) 564–569.
[9] G. Kresse, J. Hafner, Phys. Rev. B 48 (1993) 13115–13118.
[10] G. Kresse, J. Furthmüller, Comput. Mater. Sci. 6 (1996) 15–50.
[11] G. Kresse, J. Furthmüller, Phys. Rev. B 54 (1996) 11169–11186.
[12] G. Kresse, D. Joubert, Phys. Rev. B 59 (1999) 1758–1775.
[13] P.E. Blöchl, Phys. Rev. B 50 (1994) 17953–17979.
[14] J.P. Perdew, K. Burke, M. Ernzerhof, Phys. Rev. Lett. 77 (1996) 3865–3868.
[15] D. Sheppard, R. Terrell, G. Henkelman, J. Chem. Phys. 128 (2008).
[16] A. Jain, S.P. Ong, G. Hautier, W. Chen, W.D. Richards, S. Dacek, S. Cholia, D. Gunter, D. Skinner, G. Ceder, K.A. Persson, APL Mater. 1 (2013) 011002.
[17] J.A. Dean, Lange's Handbook of Chemistry, 15th ed., McGraw-Hill, New York, 1999.
[18] S.L. Shang, A. Saengdeejing, Z.G. Mei, D.E. Kim, H. Zhang, S. Ganeshan, Y. Wang, Z.K. Liu, Comput. Mater. Sci. 48 (2010) 813–826.
[19] A.E. Smith, Surf. Sci. 601 (2007) 5762–5765.
[20] Q. Zhang, T.W. Fan, L. Fu, B.Y. Tang, L.M. Peng, W.J. Ding, Intermetallics 29 (2012) 21–26.
[21] L. Wen, P. Chen, Z.F. Tong, B.Y. Tang, L.M. Peng, W.J. Ding, Eur. Phys. J. B 72 (2009) 397–403.
[22] T.W. Fan, B.Y. Tang, L.M. Peng, W.J. Ding, Scr. Mater. 64 (2011) 942–945.
[23] Y. Wang, L.Q. Chen, Z.K. Liu, S.N. Mathaudhu, Scr. Mater. 62 (2010) 646–649.
[24] M. Muzyk, Z. Pakiela, K.J. Kurzydlowski, Scr. Mater. 66 (2012) 219–222.
[25] S.L. Shang, W.Y. Wang, B.C. Zhou, Y. Wang, K.A. Darling, L.J. Kecskes, S.N. Mathaudhu, Z.K. Liu, Acta Mater. 67 (2014) 168–180.
[26] Y. Dou, J. Zhang, Comput. Mater. Sci. 98 (2015) 405–409.
[27] D. Hull, D.J. Bacon, Introduction to Dislocations, 4th ed., Butterworth-Heinemann, Woburn, 2001.